STUDY OF LITHIUM INTERCALATION IN TITANIUM DISULPHIDE USING TIME DIFFERENTIAL PERTURBED ANGULAR CORRELATIONS

by

DJOKO SURONO

B.Sc., Universitas Indonesia, 1986

A THESIS SUBMITTED IN PARTIAL FULFILLMENT OF

THE REQUIREMENTS FOR THE DEGREE OF

MASTER OF SCIENCE

in

THE FACULTY OF GRADUATE STUDIES

Departement of Physics

We accept this thesis as conforming

to the required standard

THE UNIVERSITY OF BRITISH COLUMBIA

July, 1991

In presenting this thesis in partial fulfilment of the requirements for an advanced degree at the University of British Columbia, I agree that the Library shall make it freely available for reference and study. I further agree that permission for extensive copying of this thesis for scholarly purposes may be granted by the head of my department or by his or her representatives. It is understood that copying or publication of this thesis for financial gain shall not be allowed without my written permission.

Department of Physics

The University of British Columbia
Vancouver, Canada

Date July 8, 1991

DE-6 (2/88)

Abstract

Lithium intercalation into layered compound TiS_2 was studied using time-differential perturbed angular correlations (TDPAC). Fast electrochemical intercalation was performed to bring Li atoms into the host. The probe atoms ^{181}Hf registered two nuclear quadrupole interactions corresponding to the empty host TiS_2 with quadrupole frequency ν_{q1}=461(5) MHz and a high packing density Li_xTiS_2 (x$\approx$1) compound with quadrupole frequency ν_{q2}=599(6) MHz. The contribution fractions of both interactions evolved as a function of charge transport, n_F. The second intercalation becomes dominant at $n_F > 0.3$. No evidence was found for intermediate x values.

List of Contents

List of Figures

Acknowledgement

I would like to thank Dr. Peter W. Martin for his supervision and encouragement, without which this work would not be possible. I am also indebted to Drs. Jeff Dahn, Peter Mulhern, Salah El Kateb and Mr. Dazong Li, for their suggestions and opinions in making the cell. Finally, I would like to thank the government of *Republik Indonesia* in which through the Overseas Fellowship Programe gave financial support during my study at UBC, and the World University Service of Canada, the administrator of the fellowship programme in Canada.

Chapter 1

The Intercalation Compound TiS_2

1.1 Introduction

In the past decade condensed matter physics has witnessed an ernormous upsurge of activity in the area of materials science. In particular, the class of materials known as intercalation compounds has received a great deal of attention [1]. In these systems guest atoms, or molecules, called the intercalant, can be inserted in a controlled fashion between layers of the host material. The resulting materials are of great interest for both theoretical and practical reasons. On the one hand, theorists are finding such layered compounds ideal testing grounds for theories of 2-dimensional physics. Moreover, by utilizing the staging phenomenon, whereby intercalant layers are separated by a definite number of host layers, the transformation from 2 to 3-dimensional behaviour can be studied. On the other hand, the ability to produce materials with specific, desired properties clearly offers many practical applications. Indeed, one such material, Li_xMoS_2, has already been exploited as a commercial electrical battery.[1] Consequently a great deal of experimental work has been brought to bear on the problem of characterizing these new materials, and the elucidation of the reaction mechanism by which they are produced.

In this thesis we are concerned with an investigation of the layered transition metal dichalcogenide compound, TiS_2, with Li atoms as the intercalant. A layered transition metal dichalcogenide compound refers to a chalcogen-metal-chalcogen sandwich structure. One writes MX_2, where M refers to the transition metal (Ti, V, Cr, Mn, Fe,

[1]Moly-Energy Ltd., 3985 Myrtle Rd., Burnaby, BC., Canada.

Co, etc.) and X refers to the chalcogen atom (S, Se). Each layer can be considered as a two-dimensional sheet of atoms. The X–M–X sandwiches are bound to each other by Van der Waals forces. Due to the weak nature of the forces between the sandwiches, guest atoms can be inserted into the gap; when they are extracted, the host crystal returns to the original structure. The process is called *intercalation.*

The technique used in these studies is that of time differential perturbed angular correlations (TDPAC). In TDPAC a radioactive probe nucleus, in this case ^{181}Hf, is introduced into the system under study (TiS_2) and the directional correlation of a suitable γ_1-γ_2 cascade is measured with a system of detectors. As will be explained later in Chapter 2, such a measurement of the perturbed angular correlation allows one to monitor changes in the electric field gradient (efg) within the host crystal, which can then be related to the electronic structure. We hope then to be able to answer the following questions:

- In the intercalation process for the production of Li_xTiS_2 how many and what type of sites are occupied by Li atoms ?
- Are there variations in the packing fraction p within a given layer, as has been found by Ramos et al. [2] for the Ag_xTaS_2 system ?
- Can TDPAC suggest a model for the intercalation dynamics ?

1.2 Structure of TiS_2

One usually uses the symbols A, B, C etc. and their lowercase counterparts to describe the arrangement of atoms in a layered structure. The letters A, B, C refer to the sites in the first, second and third layers of atoms respectively. As depicted in figure 1.1, type A specifies the sites of atoms in a hexagonal structure, while types B and C are

the two possible octahedral sites above the first layer. The stacking of atoms in the next layer can always be positioned in A, B, or C sites. The number of layers can be very large and depends on the size of the crystalline grain. Different atoms are distinguished by letter type (upper case, lower case, Greek letters, etc.). An AbC structure, for example, is an arrangement of two different atoms which are represented by upper and lower case letters and positioned in A, B and C sites respectively.

Transition metal dichalcogenide compounds have a hexagonal closed packed structure. In ABC notation the metal and chalcogenide atoms are represented using lower case and upper case letters respectively. There are two possible sites for the transition metal: trigonal prismatic and octahedral coordination sites. In both coordinations the metal atoms have six chalcogen nearest neighbours. These two different crystal symmetries lead to a different band structure and electronic properties [3].

A trigonal prismatic coordination is an arrangement in which the third layer of atoms lies directly above atoms in the first layer. The metal atom lies in the center of the prism (see fig. 1.1). It is written as A-b-A coordination. An octahedral coordination, on the other hand, is written as A-b-C. In this case the third layer atoms are rotated 180° about the z- axis. It is also called trigonal anti prismatic coordination. The terms 1H and 1T are also used to denote trigonal prismatic and octahedral coordination respectively. The number 1 refers to the number of layers per unit cell and the letters T and H do not represent the position of the transition metal, but relate to the whole crystal structure of the compound.

Titanium disulfide has a 1T-CdI_2 structure[2]. It is a layered A-b-C coordination of S–Ti–S. The titanium atoms occupy octahedral sites and are surrounded by six sulphur atoms. The covalent bonds in TiS_2 are relatively strong and stable, but the Van der Waals force is sufficiently weak so that the intercalation process can be performed. The

[2]This type of structure was apparently first known for CdI_2.

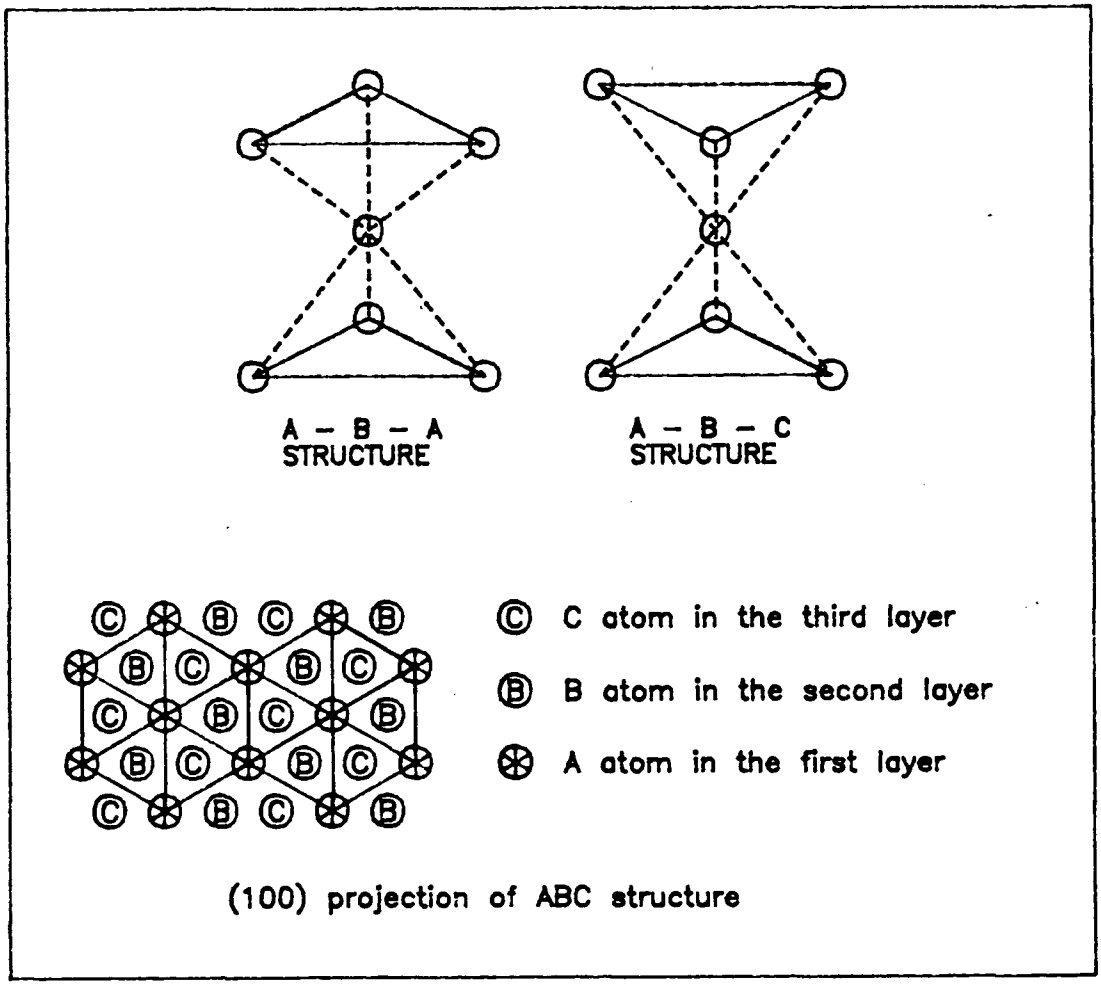

Figure 1.1: A–B–C arrangement of atoms.

reverse process, i.e. pulling guest atoms out from the crystal, is called de-intercalation.[3]

The **a** lattice parameter does not change very much in the intercalation process [5,6]. This follows from the fact that the covalent bond in TiS_2 is very stable. On the other hand, the **c** parameter varies with the content of Li in intercalated compound Li_xTiS_2. This phenomenon can only be explained if the Li atoms occupy sites within the Van der Waals gap, with a consequent change in the width of the gap.

[3]Sometimes people refer the word *intercalation* for both processes.

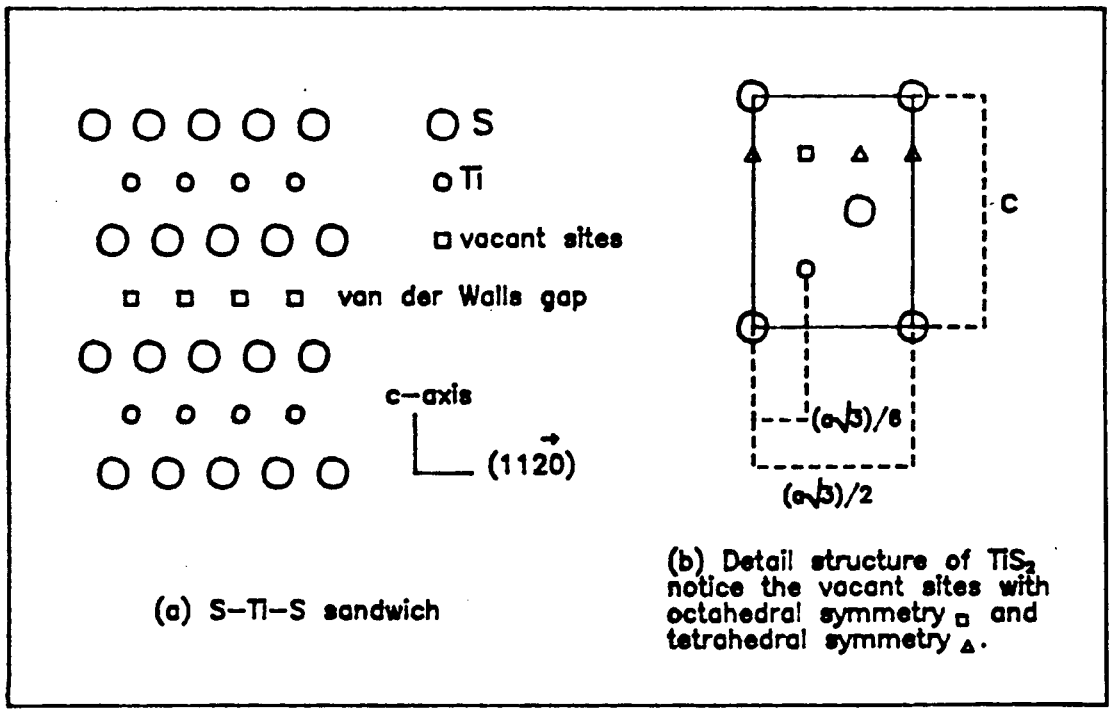

Figure 1.2: Structure of TiS_2.

There are two types of symmetry sites in the Van der Waals gap[4]: octahedral and tetragonal sites. The octahedral sites have the same nearest neighbors as the metal in the second layer (six sulphur atoms), i.e. they are similar to those occupied by Ti in the S–Ti–S sandwich. From fig. 1.2 one can see that the octahedral sites are positioned directly above Ti atoms, so that there is one octahedral site in the Van der Waals gap per TiS_2 molecule. Tetrahedral sites are the vacant sites above the third layer S atoms. There are four nearest neighbour sulphur atoms for each site and 2n sites per n TiS_2 molecules.

The octahedral site has a larger radius[5] than the tetrahedral site. For TiS_2, the radii of octahedral and tetrahedral sites are 0.89 $\AA$ and 0.64 $\AA$ respectively [1]. It would

[4]It can be considered as the fourth layer of S–Ti–S–Li sandwich

[5]The radius of a vacant site is the maximum radius of an atom which can be inserted in this site without changing the whole stucture (hard sphere ball model).

seem then that the tetrahedral site is too small for the Li^+ ion, which has radius of 0.7 Å. Previous workers (see for example [6,7]) confirm that for $0 < x \leq 1$ only octahedral sites are occupied by Li^+ ions.

For titanium disulphide Ti_yS_2, where y=1+δ (δ a small number), excess Ti atoms also occupy the vacant sites in the Van der Waals gap [8], thus reducing the number of possible intercalation sites and the rate of intercalation[6]. In contrast to the former situation where expansion of the c-axis occurs with increasing number of intercalant atoms, in this case the c-parameter decreases with increasing excess of titanium atoms, even though in both cases guest atoms reside in the gap. Whittingham [9] suggested that the strong covalent bonding of Ti to the layers was responsible for this phenomenon. Excess Ti pins the sandwiches together, so that the gap becomes narrower and more rigid. Consequently it may reduce the rate of Li diffusion into the host in electrochemical intercalation.

1.3 Electrochemical intercalation

Intercalation can be achieved using chemical (n-butyl lithiation) [9,10], electrochemical [6,7] or physical methods (temperature and pressure) [11]. In this work, only electrochemical intercalation was performed. The procedure involved charging and discharging a battery system constructed using host material as cathode and intercalant metal (Li sheet) as anode. A salt material serves as the electrolyte, transporting the metal intercalant into the host.

The intercalation process is based on a simple electrochemical reaction,

$$xT \rightleftharpoons xT^{z+} + xze^- \tag{1.1}$$

$$xT^{z+} + xze^- + MN_2 \rightleftharpoons T_xMN_2 \tag{1.2}$$

[6]In this work Thompson used the n-butyl lithiation method to intercalate TiS_2.

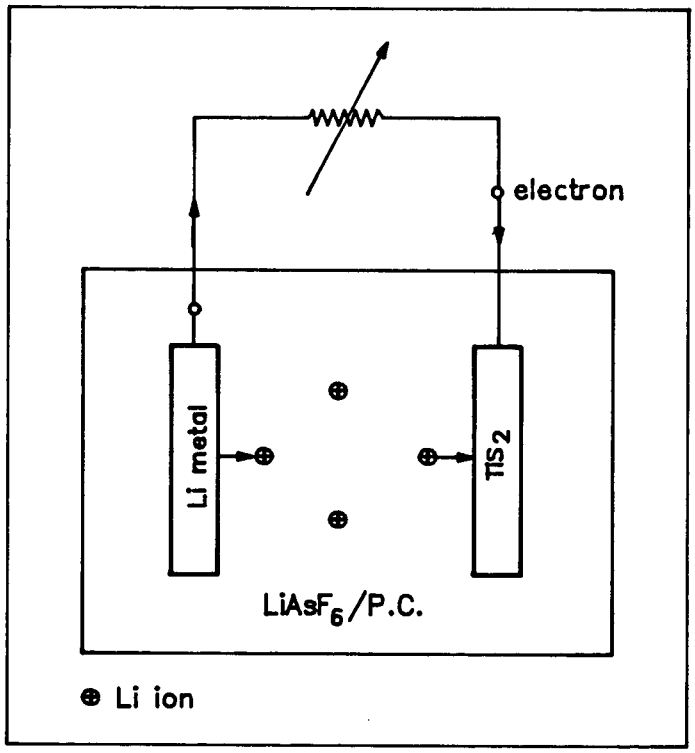

Figure 1.3: Diagram of an electrochemical prosess (discharge). The Li metal and TiS_2 compound are used as cathode and anode respectively. The electrolyte used is $LiAsF_6$ in Propylene Carbonate.

The number of guest atoms, T, intercalated into the host material, MN_2, is proportional to the charge transport.

As shown in the diagram (fig. 1.3), electrons travel from cathode to anode via an external circuit, while metal ions are transported through the electrolyte. There is no external voltage needed in the intercalation process; chemical potential difference serves as a driving force. The reverse process, de- intercalation, can be achieved by applying external voltage to the cell (charging the cell). The amount of charge transported is measured from the external current.

The molar fraction, x, can simply be calculated if the mass, m, of the cathode material, the external current, I, and the period of time for the process, t, are all known.

Let N be the number of molecules, N=mN_0/M, where N_0 is Avogadro number ($N_0 = 6.02 \times 10^{23}$) and M is the molecular wieght of the cathode material. The total charge transported is Q=I×t. The number of guest atoms intercalated can be written as $N_x = Q/(z \times e^-)$, where z is the valence of the guest atoms. The mole fraction x is equal to the ratio of the number of guest atoms transferred, N_x, and the number of the host molecules N; it can be written as

$$\begin{aligned} x &= \frac{N_x}{N} \\ &= \frac{QM}{zme^-N_0} \\ &= \frac{ItM}{zmF} \end{aligned} \tag{1.3}$$

where F is known as the Faraday constant and the equation is called Faraday's law. In the above calculation one has assumed that the guest atoms are distributed homogeneously throughout the entire crystalline host.

The fraction x generally refers to the average molar composition. One may prefer using *charge transport*, n_F, to indicate the molar fraction in electrochemical intercalation. Charge transport[7] n_F is defined as the number of electrons transported from anode to cathode via an external circuit, divided by the number of molecules of cathode material.

$$\begin{aligned} n_F &= \frac{Q/e^-}{N} \\ &= xz \end{aligned} \tag{1.4}$$

For z=1 (such as Li), the molar fraction is equal to the charge transport, $x = n_F$.

In TDPAC measurements one is interested in the amount of charge transferred from intercalated atoms to the host crystal, as this will contribute to the changes in the electric field gradient (efg) within the host. For this reason one defines a new parameter, the

[7]The letter F in n_F indicates that this parameter is calculated from Faraday's law

charge transfer n_L (L refers to metal intercalant Li, Ag, etc.), as the number of electrons transferred from the intercalated metal to the host per number of host molecules. For empty host material n_L=0, and in general $0 \leq n_L \leq s$, where s is the maximum uptake.

The charge transfer parameter can not be determined theoretically. Its value depends on the quality of the sample used and cell performance. It indicates the local concentration of intercalated metal in the host, so that a sample (the material used as cathode of the cell) may have several values of n_L in the case of non-homogeneous intercalation. In this case one may prefer using *packing fraction* p instead of the global molar fraction x. The packing fraction is defined as the number of intercalated atoms per molecule; it refers to the local concentration of intercalated metal in the host crystal, and could vary even within a given layer.

In an ideal situation in which the intercalated atoms are distributed homogeneously and transfer their charge properly, all of the four parameters above have a simple relation, viz. $x = p = n_F/z = n_L/z$. In the special case when the valence number of the intercalated atom is z=1, all these quantities have the same value.

In the following chapter the theory of TDPAC will be presented briefly. Details of the electrochemical intercalation experiment and a brief description of the TDPAC detector system used can be found in Chapter 3. Results of the experiment and their interpretation are presented in Chapters 4 and 5. In Chapter 6 we draw some conclusions and give some suggestions for future work to improve our understanding of layered compound systems.

Chapter 2

Theory of Time Differential Perturbed Angular Correlation

2.1 Introduction

A brief description of the theory of angular correlations is presented here. A detailed account can be found in the review article by Frauenfelder and Steffen [13]. It is well known that a randomly oriented radioactive material emits particles or γ-rays isotropically. The intensity of radiation depends on the strength (activity) of the source, the distance and nature of the medium between the source and the detector. Since there is no preferred direction, i.e. the z- axis is arbitrary, it does not depend on the angle the detector makes with the z-axis. If, however, the nuclear spin is somehow aligned preferentially with respect to the z-axis (for example by low temperature nuclear orientation, or by the application of an extremely intense electric or magnetic field), it can be shown that as a consequence of angular momentum conservation, the nuclear radiation will in general exhibit a definite angular distribution with respect to the quantization axis.

Consider for an example an unstable nucleus in a state characterized by spin angular momentum numbers (I_i, m_i). It decays to a state (I_f, m_f) and the emitted γ-ray has quantum numbers (L,M). For the angular momentum to be conserved, one has to have $\overline{I_i} = \overline{L} + \overline{I_f}$ and $m_i = M + m_f$. The magnetic quantum number M is defined as $L_z = M\hbar$, where L_z is the projection of $\overline{L}$ on an arbitrary quantization axis (z-axis). The probability distribution of the emitted γ-ray is characterized by a directional distribution function $F_M^L(\theta)$, where θ is the angle between the z-axis and the emitted γ-ray. This function

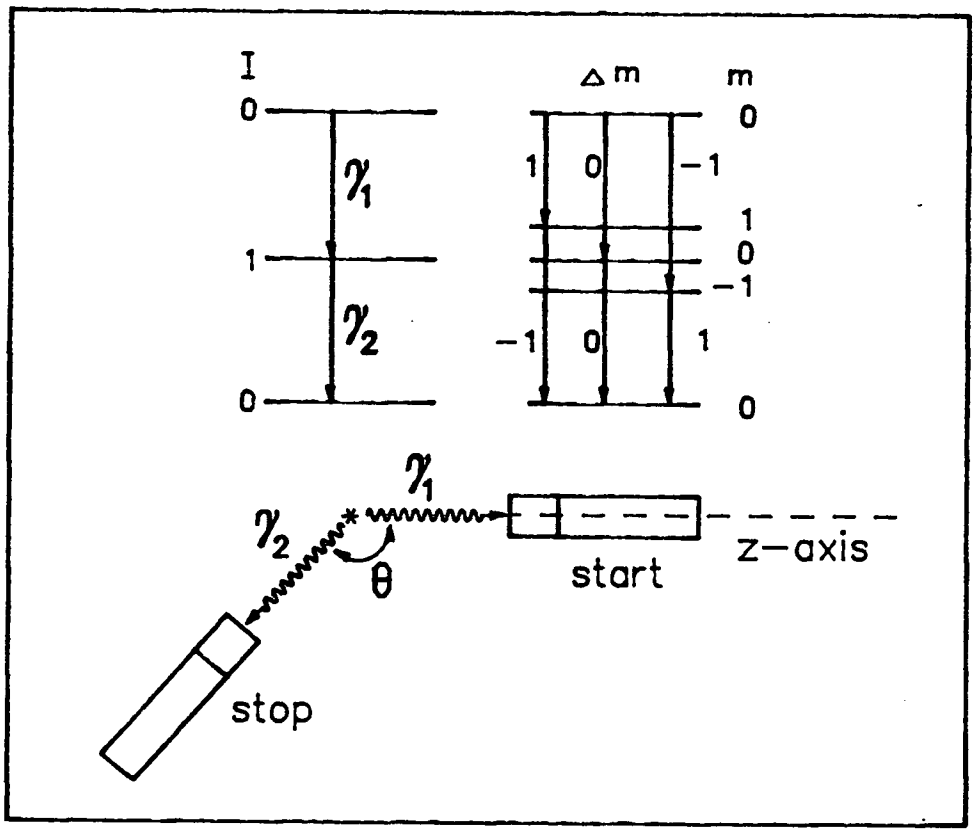

Figure 2.1: A successive dipole transition with I: $0 \rightarrow 1 \rightarrow 0$ and the possible values of m and Δm (a); schematic diagram of an angular correlation experiment (b).

depends on the values of L and M, but not on the initial or final state spins. For the well known case of dipole radiation, for example, the probability distribution functions are given by:

$$F_0^1(\theta) = C\sin^2(\theta); \quad F_{\pm 1}^1 = \frac{C}{2}\{1 + cos^2(\theta)\}$$

where C is a constant.

In the language of quantum mechanics we can say that preferential alignment of the nuclear spins is achieved when the magnetic substates of the initial state are not evenly populated. In the case of low temperature nuclear orientation this is achieved through the Boltzmann factor, $\exp(-\mu B/kT)$, by generating large magnetic fields ($\sim$ 10 - 50 T)

at very low temperatures ($\sim$ mK).

The need to produce large magnetic fields at such low temperatures is circumvented by TDPAC, whereby successive γ-rays in a suitable nuclear cascade are detected in coincidence. In this case the detection of the first γ-ray serves as a quantum state selector for the intermediate state, producing a preferential population of its magnetic substates, with the result that the second transition will (in general) exhibit a directional correlation with respect to the first.

This can be demonstrated readily by the following example indicated in figure 2.4, which shows successive dipole transitions for the $0 \rightarrow 1 \rightarrow 0$ spin sequence. If the γ_1 transition is not detected, i.e. we just detect the singles corresponding to γ_2, we obtain the expected isotropic distribution for γ_2, viz.

$$\begin{aligned} W(\theta) &= \sum_m p_m F_m^L(\theta) \\ &= F_0^1(\theta) + 2F_{\pm 1}^1(\theta) \\ &= C sin^2(\theta) + 2\frac{C}{2}\{1 + cos^2(\theta)\} \\ &= constant \quad (i.e.\ isotropic) \end{aligned}$$

where p_m are the (equal) relative populations of the magnetic sublevels.

Suppose now we arbitrarily choose the direction of γ_1 as the z-axis, noting, however, that there is zero probability for emission of the Δm=0 transition in this direction, since $F_0^1 \sim \sin^2(\theta)$. The probability of detecting γ_1 and γ_2 in coincidence is now :

$$\begin{aligned} W(\theta) &= \sum_m p_m F_m^L(\theta) \qquad (with \quad p_0 = 0) \\ &= C\{1 + cos^2(\theta)\} \end{aligned} \tag{2.5}$$

so that the correlation is no longer isotropic.

Typically the situation is more complex than this example, but the principle is the same. For the more general situation depicted in figure (2.5) it can be shown that the

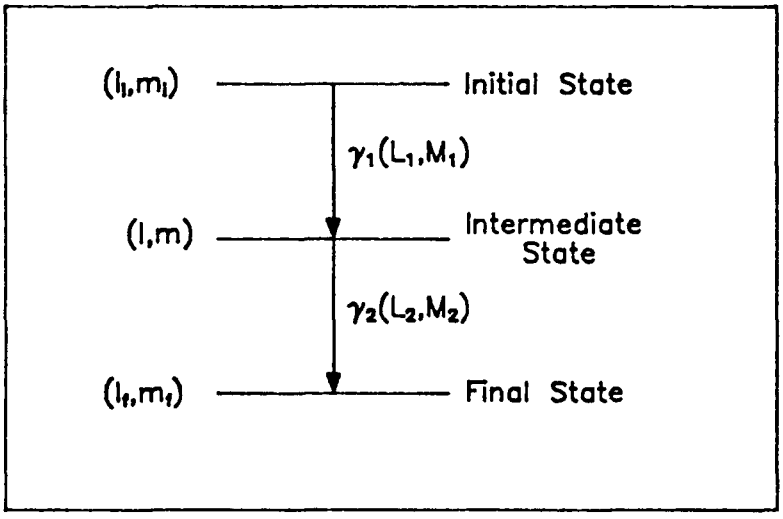

Figure 2.2: Schematic of a quantum nuclear states connected by a γ-γ cascade.

angular correlation function for a randomly oriented ensemble of nuclei can be expressed as :

$$W(\theta) = \frac{1}{4\pi\tau_N} \sum_{k=0,2,4}^{k_{max}} A_{kk} P_k(cos\theta) \tag{2.2}$$

where τ_N is the life time of the intermediate state. Conservation of parity demands only even values for the index k, with a maximum value determined by angular momentum conservation :

$$k_{max} = Min(2I, 2L_1, 2L_2). \tag{2.3}$$

The parameters A_{kk} are real numbers called radiation parameters. They involve the product of two parameters, $A_k(1)$ and $A_k(2)$, originating from the first and second transitions respectively,

$$A_{kk} = A_k(1) \times A_k(2). \tag{2.4}$$

One can calculate the values of A_k(i) theoretically if all quantum numbers and mixing ratios involved in the cascade are known. Conversely, A_{kk} can be determined by measuring $W(\theta)$ in an angular correlation experiment so that information about nuclear properties can be extracted.

2.2 The Perturbed Angular Correlation

Expression (2.6) assumes that the nucleus is in a field free environment with a negligibly short lifetime in the intermediate state. If the intermediate state has a life time, τ_N, interactions can then occur between the multipole moments (e.g. magnetic dipole, electric quadrupole) of the state and the local electromagnetic environment (magnetic field, efg). Such interactions can induce transitions between the substates of the intermediate level, resulting in a redistribution of the populations and consequently a perturbation of the correlation function in eq.(2.5). The latter can be written as

$$W(\theta,t) = \frac{1}{4\pi\tau_N}\sum A_{kk}G_{kk}(t)P_k(cos\theta) \tag{2.9}$$

where G_{kk}(t) is the *perturbation factor.*

Measurement of the latter is the primary goal of TDPAC. The form of $G_{kk}(t)$ depends on the type of interaction causing the perturbation. Thus TDPAC is an *environmental* technique, since the determination of the pertubartion factor yields information about the probe's electromagnetic environment, which in turn relates to the electronic structure of the material.

2.3 Nuclear Quadrupole Interaction

In this work we are concerned primarily with nuclear quadrupole interactions (NQI). A static efg from surrounding atoms causes a splitting in the intermediate nuclear state. The situation is shown in fig.(2.6) for the case of spin I=5/2.

For an axially symmetric efg, the energy eigenvalues of the substates m are

$$E_m = e^2qQ\frac{3m^2 - I(I-1)}{4I(2I-1)}. \tag{2.10}$$

Here eQ is the nuclear quadrupole moment and eq is the largest component of the efg tensor (V_{zz}). I and m are the quantum numbers of the intermediate state.

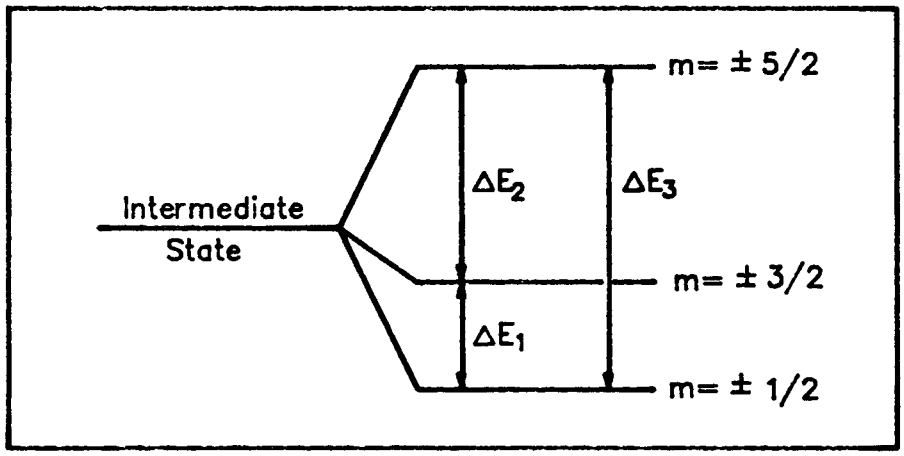

Figure 2.3: Splitting of the intermediate state due to a symmetric efg.

The electric field gradient is a traceless tensor and can be written as

$$V = \begin{pmatrix} V_{xx} & 0 & 0 \\ 0 & V_{yy} & 0 \\ 0 & 0 & V_{zz} \end{pmatrix} \quad where\ V_{xx} + V_{yy} + V_{zz} = 0.$$

For the non-symmetric case one can define the asymmetry parameter as

$$\eta = \frac{|(V_{xx} - V_{yy})|}{V_{zz}}. \tag{2.7}$$

Clearly, $0 < \eta < 1$ for $V_{zz} \geq V_{xx} \geq V_{yy}$. It equals zero (symmetric efg) only if V_{xx}=V_{yy}.

The energy difference between sublevels m can be calculated from equation (2.6) :

$$\Delta E_{m,m'} = \frac{3(m^2 - m'^2)}{4I(2I-1)} eQV_{zz}. \tag{2.8}$$

One defines the angular frequency ω_0 corresponding to the smallest energy difference by

$$\Delta E_{m,m'} = \hbar\omega_0 \tag{2.9}$$

and the *quadrupole frequency* by,

$$\nu_q = \frac{eQV_{zz}}{h}. \tag{2.10}$$

For the case of axial symmetry, the smallest energy difference is equivalent to $h\nu_1$, where ν_1 is the first harmonic of the interaction. For $I = \frac{5}{2}$ one writes

$$\begin{aligned} \Delta E_1 &= \Delta E_{\pm\frac{3}{2},\pm\frac{1}{2}} \\ h\nu_1 &= \frac{6}{40} eQV_{zz}, \end{aligned}$$

then from eq.(2.14) we have

$$\nu_q = \frac{40}{6}\nu_1. \tag{2.15}$$

However, in terms of the fundamental (angular) frequency, ω_0, where $\Delta E_1 = \hbar\omega_0$, we have

$$\omega_0 = \frac{3\pi}{10}\nu_q. \tag{2.16}$$

Similarly it can be shown that $\Delta E_2 = 2\hbar\omega_0$ and $\Delta E_3 = 3\hbar\omega_0$ respectiveley. For the case of ^{181}Ta, the daughter product in the decay of ^{181}Hf, terms in k>2 are negligible, and the perturbation factor in this case is (I=5/2, η=0, randomly oriented sample) :

$$G_{22}(t) = S_0 + \sum_{n=1}^{3} S_n cos(\omega_n t) \tag{2.17}$$

where $\omega_n = n\omega_0$ (n=1,2,3).

For the case $\eta \neq 0$, the quadrupole frequencies no longer form a harmonic series. Now we must write

$$\omega_n = f(\eta)\omega_0 \tag{2.18}$$

where the coefficients $f(\eta)$ are calculable functions of η.

2.4 Correction for Broadening Mechanisms

The expression in eq.(2.17) must be corrected for various broadening mechanisms before the theory can be compared with experimental data. Details on the experimental procedure and data reduction methodology will be discussed in Chapter 3.

Since the detectors subtend a finite solid angle, the radiation parameters A_{kk} must be corrected accordingly [13]. We write

$$A_k^{corr.}(1) = Q_k(E_{\gamma_1})A_k(1) \tag{2.19}$$

and a similar expression for $A_k^{corr.}(2)$. The solid angle correction factors were calculated using the routine DEWF [13].

As the fast coincidence circuit is limited by its finite resolving time (FWHM=τ_R), the perturbation factor must also be multiplied by a factor $\exp(-\frac{1}{2}\omega_n^2\sigma^2)$, where we have assumed a Gaussian spread with standard deviation σ, with

$$\tau_R = 2\sqrt{2}\sqrt{\ln 2}\sigma. \tag{2.20}$$

Finally, owing to imperfections in the crystal lattice, not all nuclei will experience the same efg, but will see some Gaussian distribution δ in the quadrupole interaction. The correction factor in this case takes the form $\exp(-\frac{1}{2}\omega_n^2\delta^2t^2)$.

Chapter 3

Experiment

3.1 Sample preparation

Production of titanium disulphide (TiS_2) can be performed using several methods. The most simple one is by placing stoichiometric ratios of titanium and sulphur in a quartz tube and then heating to 600–1000 ^{0}C. The tube has to be evacuated to avoid oxidation. Dahn [6] reported formation of several crystallite sizes depending on the baking temperatures. Single crystals of TiS_2 can be produced using the iodine vapour transport method.

The titanium disulphide used in this work was prepared using the stoichiometric method. A small amount of high purity hafnium was added as a probe atom for the TDPAC measurements. The final sample was determined to be $Hf_{0.0097}Ti_{0.9903}S_{2.0000}$, a golden brown metallic powder. The sample had to be ground to get a uniform crystallite size with an average diameter of 40 μm.

An X-ray analysis was performed before the sample could be used as cathode material. The X-ray pattern of the sample was well matched with the standard X-ray diffraction pattern of TiS_2 as shown in figure 3.7. This constituted a preliminary check of the sample before it could be used as cathode material for the Li/Li_xTiS_2 electrochemical cell.

The isotope required for the angular correlation experiments was ^{181}Hf. A 10–12 mg sample of $Hf_{0.0097}Ti_{0.9903}S_{2.0000}$ was placed in a small quartz tube, about 4 mm in

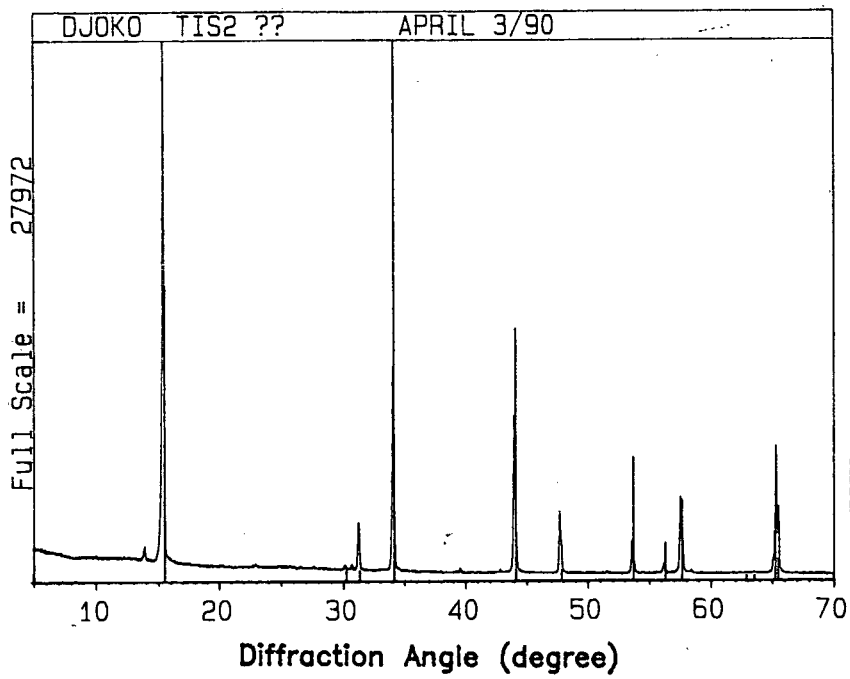

Figure 3.1: X-ray diffraction pattern of the TiS_2 sample used (red pen); the green pen is the calculated spectrum.

diameter, sealed and sent to Mc Master University to be neutron irradiated. The resulting activity of the sample was approximately 10 μCi.

As the thermal neutron absorption cross section for hafnium is very high (12.2 b), it was expected that radiation damage to the sample would be negligible. However, the results of this work revealed drastic differences in TDPAC spectra (G_{22} vs. time) for samples with and without further treatment after being neutron irradiated. Further discussion on radiation damage and possible treatment can be found in Chapter 4.

3.2 Design of the electrochemical cell

The design of cells used in this work is similar to that used by previous workers [3,6]. However, some changes in the design of the cell were required to minimize the effect of γ-ray absorption so that the cell could be used in TDPAC measurements.

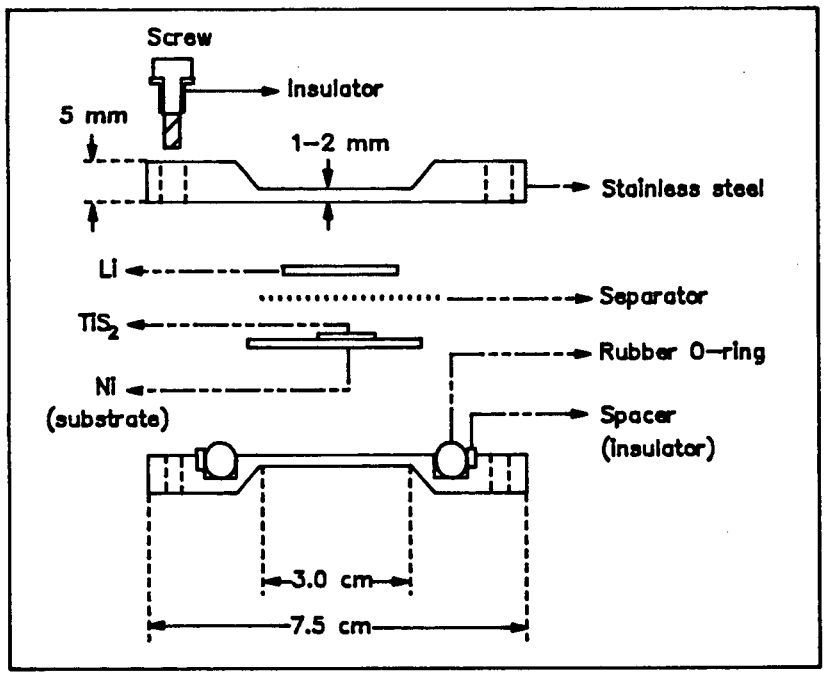

Figure 3.2: Diagram of the electrochemical cell.

Basically the cell used here consisted of two stainless steel flanges as the main body. They are joined together by six insulated metal screws (see fig. 3.2), but separated from each other by an O–ring to avoid direct contact. The intercalation process taking place inside the flanges was thus isolated from the atmosphere. The flanges also served as electrical contacts. Assembly of the cell was performed in a glove box under a clean (Argon) atmosphere.

The central part of the flanges had to be made as thin as possible to minimize γ-ray absorption. However, care had to be taken in designing the flanges since they still had to be strong enough to support the whole assembly and exert uniform pressure over the area of the sample. A schematic diagram of the flanges can be seen in fig. 3.2.

The electrolyte used in this work was 1M Lithium Hexafluor Arsenate ($LiAsF_6$) in propylene carbonate (PC). It was supplied by Moly Energy Co.[1] Water and propylene

[1]Thanks to Dr. J.R.Dahn who supplied the electrolyte.

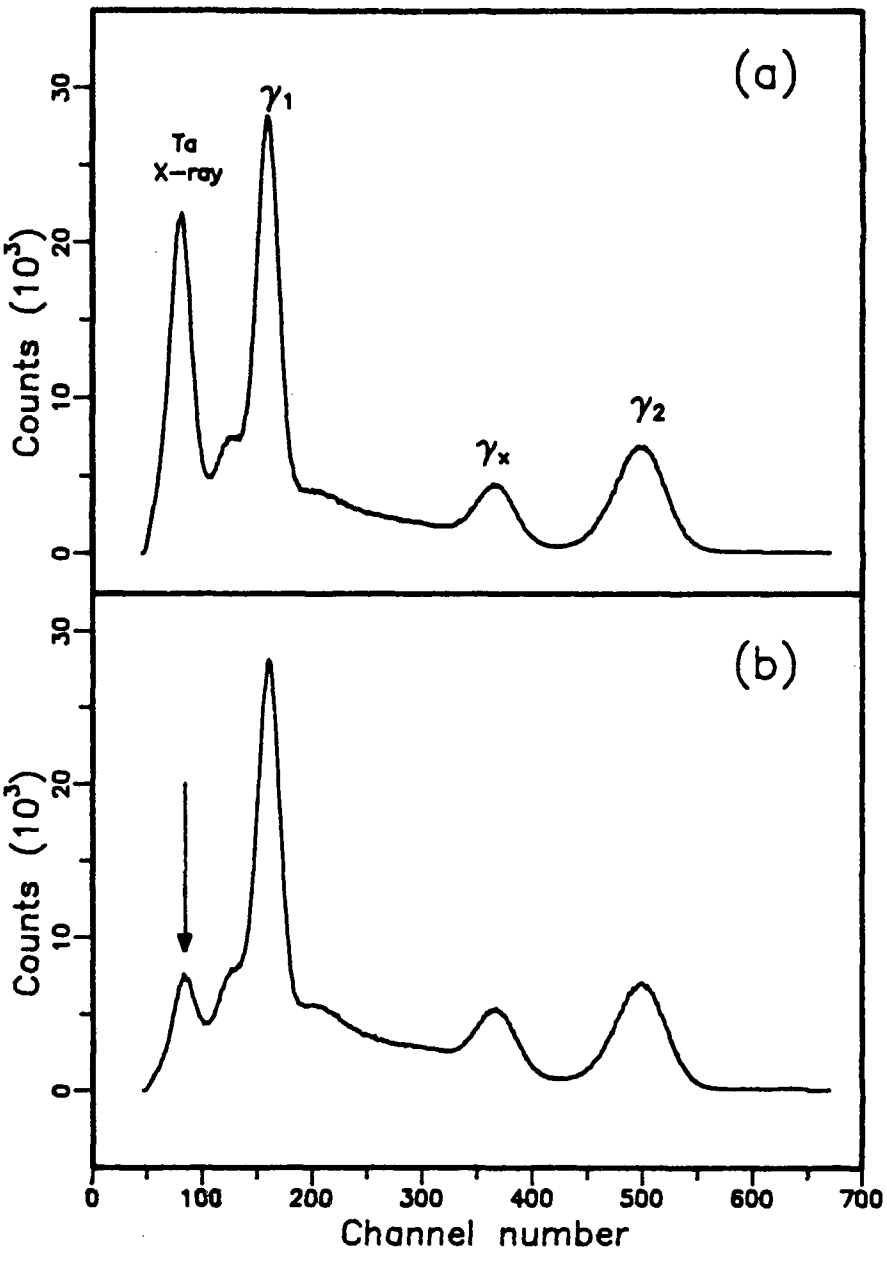

Figure 3.3: Gamma-ray spectra of ^{181}Hf, $E_{\gamma 1}$=133 keV, $E_{\gamma 2}$=482 keV and $E_{\gamma x}$=346 keV; the γ_x is not involved in the cascade of interest (see fig. 3.4). (a) The sample was placed in a pyrex tube. (b) Hf spectra of Li/Li_xTiS_2 cell. The Ta X-ray peak (E_{X-ray} = 57 keV) was absorbed by the stainless steel flanges (arrowed).

glycol content was less than 20 ppm. A Celgrad Microporus Film (product type #3501) was used as a separator. This material permits ionic contact between anode and cathode via the electrolyte, but on the other hand prevents direct electrical contact. A 0.25 mm thick lithium foil from Foote Mineral Company was used as the metal intercalant (anode). The cell was constructed as follows : (i) outside the glove box, the cathode was made by placing the TiS_2 powder on a nickel sheet which had been etched in nitric acid and rinsed using destilled water. A few drops of solvent (cyclohexane) were then added. By properly mixing the powder and the solvent, the powder sticks to the nickel sheet after the solvent evaporates; (ii) the anode was made by cutting the Li foil to about 1.5–2 cm in diameter; (iii) the whole cell was fabricated by adding a few drops of electrolyte to the cathode and then constructing a sandwich of cathode-separator-anode as depicted in fig.3.8. Steps (ii) and (iii) were performed in the glove box.

It has been mentioned previously that the flanges of the cell should be as thin as possible to minimize γ-ray absorption, but still thick enough to provide mechanical robustness. Figure 3.9 shows that the effects of absorbtion by the flanges on the γ-rays of interest (133 keV and 482 keV) are negligible. In fact it can be seen that the stainlees steel confers a distinct advantage by preferentially absorbing the low energy Tantalum X-ray at 57 keV. This is presumably a result of resonant absorption by Ta atoms in the stainless steel. The elimination of such unwanted signals is of particular advantage in lowering the count rate in the time-to- amplitude converter, with a corresponding decrease in the random background.

3.3 Time Differential Perturbed Angular Correlation Experiment

This work was performed using the four detector system described by Martin et al. [14]. Each detector consi[illegible] a NaI crystal (4.41 cm diameter, 1.27 cm and

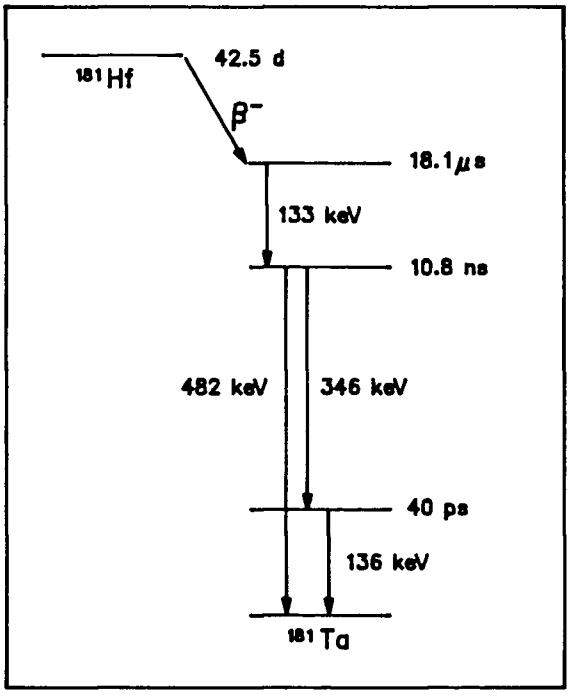

Figure 3.4: The decay scheme of ^{181}Hf.

5.08 cm thick for the start and stop detectors respectively) mounted on Philips 56 AVP photomultipliers. The axes of these detectors were set perpendicular to each other. There were four pairs of start-stop detectors: AB(π), AC($\frac{\pi}{2}$), DC(π) and DB($\frac{\pi}{2}$). The configuration of the detectors can be seen in figure 3.5.

As mentioned earlier, the isotope used for the TDPAC measurements was ^{181}Hf. Figure 3.4 shows the decay scheme of ^{181}Hf. Following β-decay to the 18 μs isomeric state of the daughter product, ^{181}Ta, the electronic shells have plenty of time to establish equilibrium before the ensuing γ-γ cascade of interest, in this case the 133 keV (start) and 482 keV (stop) transitions. Each detector produces a fast and a slow signal. The fast signals are required for precise timing measurements, while the slow signals are used in logic circuits to analyze the γ-rays i.e. to select by energy those γ-rays involved in the cascade and to determine (by a slow coincidence requirement) from which pair of detectors each event originated.

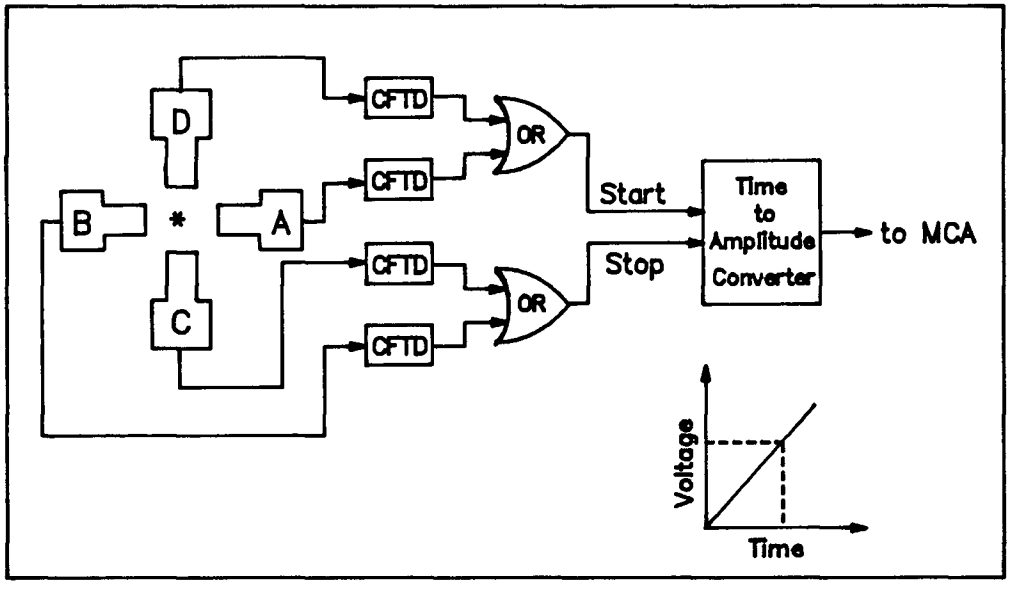

Figure 3.5: Schematic diagram of fast electronic circuit (based on Martin et al. [14]).

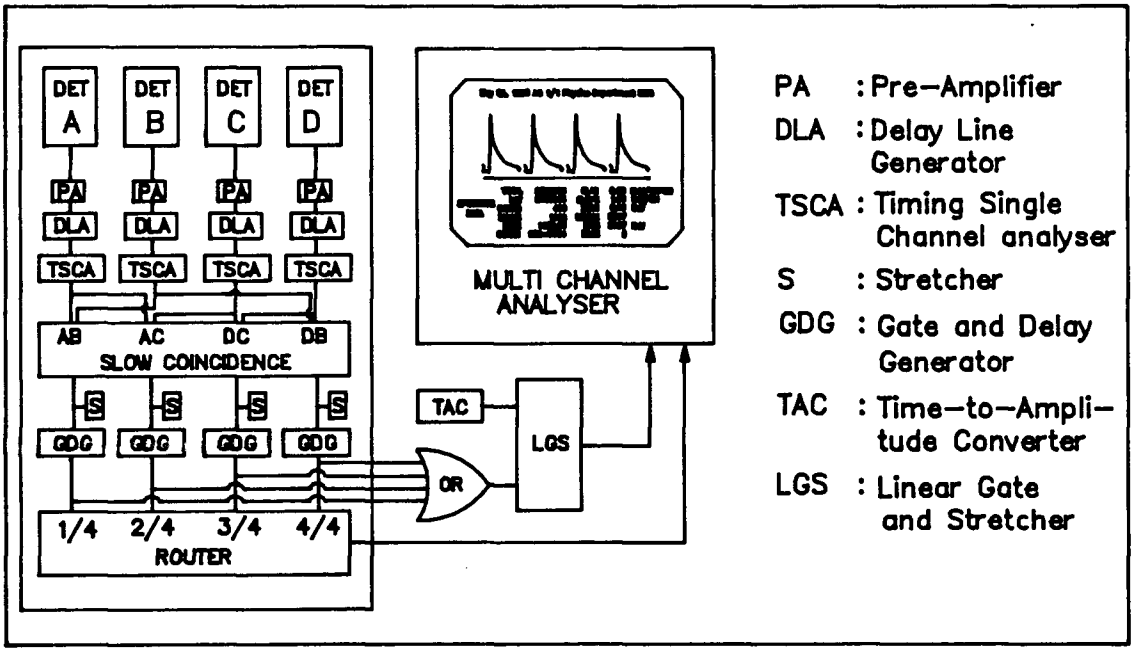

Figure 3.6: Slow electronic circuit diagram of a four detector system TDPAC (based on Martin et al. [14]).

Each fast output signal is first sent to a discriminator in order to generate a standard logic signal. A constant fraction timing discriminator (CFTD figure 3.11) produces the needed signal with minimum *walk*. It accomplishes this by triggering at a constant fraction of maximum amplitude of the input signals, consequently producing more precise timing measurements.

Start signals from detector A and D and stop signals from detectors B and C enter the time-to-amplitude converter (TAC) via an *OR* circuit. The voltage output of the TAC is proportional to the time delay between the arrival of the first and second γ-rays. This information is finally presented to the MCA after passing through a linear gate.

The gating signal for the latter is generated by the slow logic (see figure (3.12). After being amplified and delayed, the slow signals are passed to single channel analysers (SCA's) which impose energy selection on the γ-rays involved in the cascade. If a true start-stop event occurs, the slow coincidence circuit then generates a signal and sends the information to a router and to the MCA. The router directs the MCA to register any event in designated quadrants of the MCA memory.

The MCA used in this work was a Nuclear Data model ND76. It has 8192 channels which can be subdivided into two groups of 4096 channels. Each group contains four quadrants of 1024 channels. The first 300 channels were usually used to store the time-uncorrelated random background. The zero time and the system resolving time were determined using a prompt source, such as ^{60}Co or ^{22}Na, with the windows in the side channels set for the γ-rays of interest. The resolution was found to be 2.2 ns (FWHM). Data were stored in the next 500-600 channels; beyond this point the data (i.e. event numbers) were comparable to the background level and not used.

In order to get relatively good data we ran each measurement for about two days of data collection time; this was repeated two or three times to get better statistics and to check reproducibility. The perturbation factor, G_{22}, was calculated for each run, then

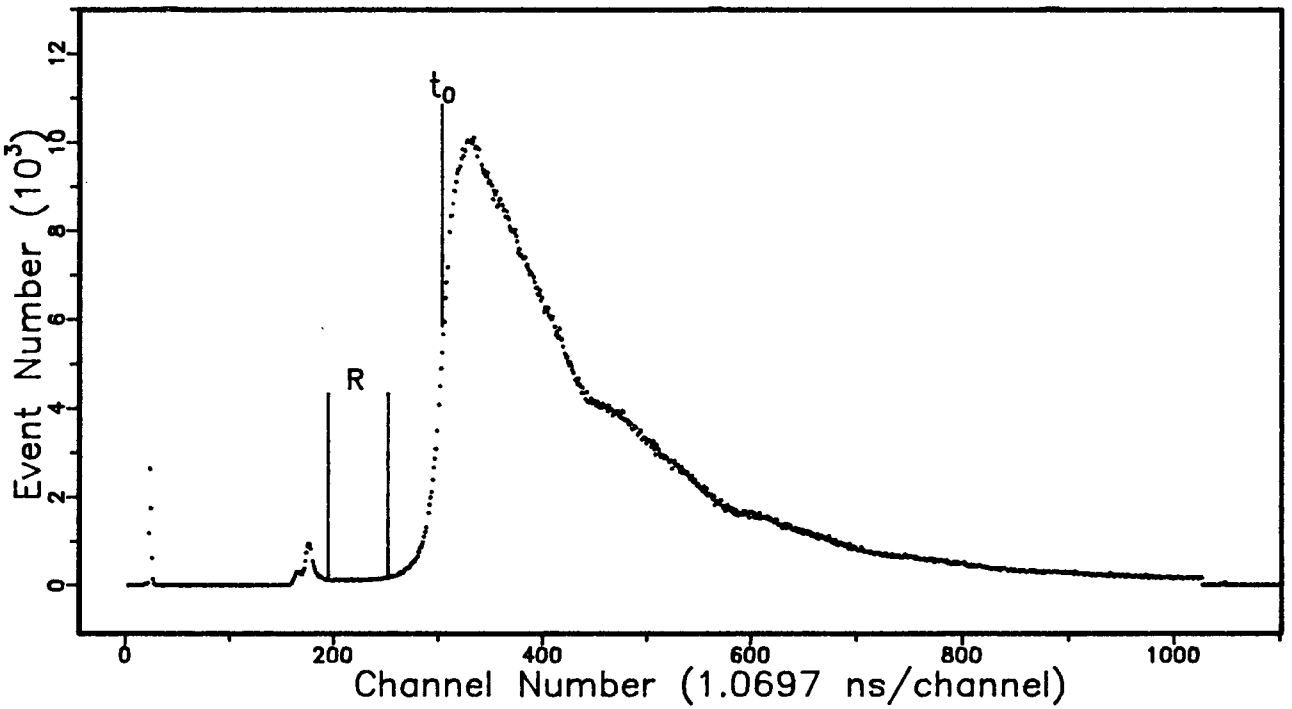

Figure 3.7 : A typical raw time spectrum of a TDPAC measurement for an annealed sample. The region labelled R corresponds to the random background. The time zero, t_0, was determined from the prompt peak using ^{22}Na as a source.

individual runs summed to obtain the weighted average. The summed data were then used in the fitting procedure. The total time needed for one sample (or for one x value in Li_xTiS_2) was about one week.

3.4 Data reduction method

The raw data of the TDPAC measurements comprised four delayed coincidence spectra (event number vs. time) originating from the AB, AC, DC and DB detectors. Figure 3.7 shows such a time spectrum from the AB detectors for the annealed sample (see Chapter 4). The time zero, t_0, was determined using ^{22}Na as a prompt source. The background level per channel was calculated from region R (see fig. 3.7) and then subtracted.

The experimental $G_{22}(t)$ function was determined from the following expression :

$$G_{22}(t) = \frac{2}{3A_{22}}\{[\frac{W_{AB}(\pi,t)W_{CD}(\pi,t)}{W_{AD}(\frac{\pi}{2},t)W_{CB}(\frac{\pi}{2},t)}]^{\frac{1}{2}} - 1\} \tag{3.21}$$

with the A_{22} parameter corrected for solid angle effects as described earlier. Here $W_{IJ}(\theta,t)$ is the true coincidence number i.e. the event number minus background for detector IJ (IJ= AB, CD, AD, or CB). This method of data reduction using a multidetector system has several advantages : (i) higher data acquisition rates; (ii) compensation of errors in source centering (owing to the symmetric positioning of the detectors); (iii) to first order a cancellation in the detector efficiencies in expression (3.21) and removal of the exponential envelope in eq. (2.5).

The G_{22} calculated using the above equation represents the total G_{22} i.e. a superposition of perturbation functions originating from several crystalline surroundings. The probe ^{181}Hf atoms may reside in several sites, each with a particular local environment corresponding to a specific NQI. Details of the data analysis and fitting procedure will be discussed in the next chapter.

Chapter 4

Results

4.1 The electrochemical cell

Investigations on Li_xTiS_2 compound which have been performed by many previous workers (Whittingham [1], Dahn et al [4,15], Thompson [7], for examples) are mainly based on voltametry, V vs. x relation. In the following section a brief résumé is given of their results and suggestions, with a view to understanding the results of this work.

Thompson claimed to observe a Li–ordering due to the long range repulsive Coulomb interaction [7]. He suggested that the intercalated Li atoms transfer their valence electrons to the host. The corresponding Li^+ ions are constrained to reside in certain octahedral sites in the gap and form a two-dimensional ordered structure. The occupation of octahedral sites by Li atoms was also confirmed by Dahn [6] for x in the range of $0 \leq x \leq 1$. On the other hand, his neutron scattering data definitely excluded three dimensional ordering, and was unable to confirm the existence of a two-dimensionally ordered structure.

The structure of Li_xTiS_2 depends on the molar fraction x. Neutron and X-ray investigations [6,16] give a_0=3.407 $\AA$ and c_0=5.696 $\AA$ for empty host TiS_2. Both parameters increase monotonically with x. The **a** lattice parameter seems to be more stable and rigid than the **c** parameter. It changes only by about 2% from x=0 to x=1.0, while **c** changes by 10%. This is consistent with the formation of a sub-layer in the Van der Waals gap, whereby the width of the gap increases with little change in the structure of

atoms parallel to the plane.

The voltage of the cells used in this work varies with n_F in a manner similar to that observed by other experimenters. The tenth continuous charge–discharge cycle of cell JK10 can be seen in figure 4.13. The current used was 50 μA, which corresponds to an intercalation rate of 12.3 hours.[1] Figure 4.13.b represents the V–x relation of cell R7. The intercalation was interrupted at points x=0.3, 0.5, 0.7 to allow TDPAC measurements; the interruptions were about 6 days for each point. All the TDPAC measurements in this work were performed using cells R5, R6 and R7. All cells exhibited similar performance to that shown in figure 4.13.b.

In figure 4.13.b, cell R7 was discharged at I=500 μA (intercalation rate = 4.73 hours) to x=0.3; the voltage dropped to 1.91 Volt. The cell was then left in the open circuit condition to allow TDPAC measurements. The voltage recovered to 2.2 Volt in an hour and slowly increased continuously during the TDPAC measurements. After one week the cell voltage was found to be 2.3 Volt. Then the cell was discharged at I=300 μA to the next points of interest, x=0.5, 0.7 and 0.9. A similar procedure was followed for cell R5; cell R6 was used for the x=0.1 measurement only.

Fast intercalation in the first discharge (i.e. using relatively high current) was aimed to avoid solvent co- intercalation.[2] As a result, the voltage was found to decrease faster than that found by Thompson [7], for example. In the case of a fast discharge, Li^+ ions are deposited on the surface of the cathode material thus preventing further deposition and solvent co-intercalation processes. It would appear that the diffusion rate of Li^+ is slower than the rate of electrochemical reaction.

The voltage of the cell recovers after the cell is disconnected. The deposited Li atoms diffuse into the host crystal so that the packing density of Li atoms in the surface

[1]The intercalation rate is the time required to change the mole fraction x by Δx=1.

[2]Solvent co-intercalation is a spontaneous intercalation by the solvent molecules, see Dahn [6] for detail.

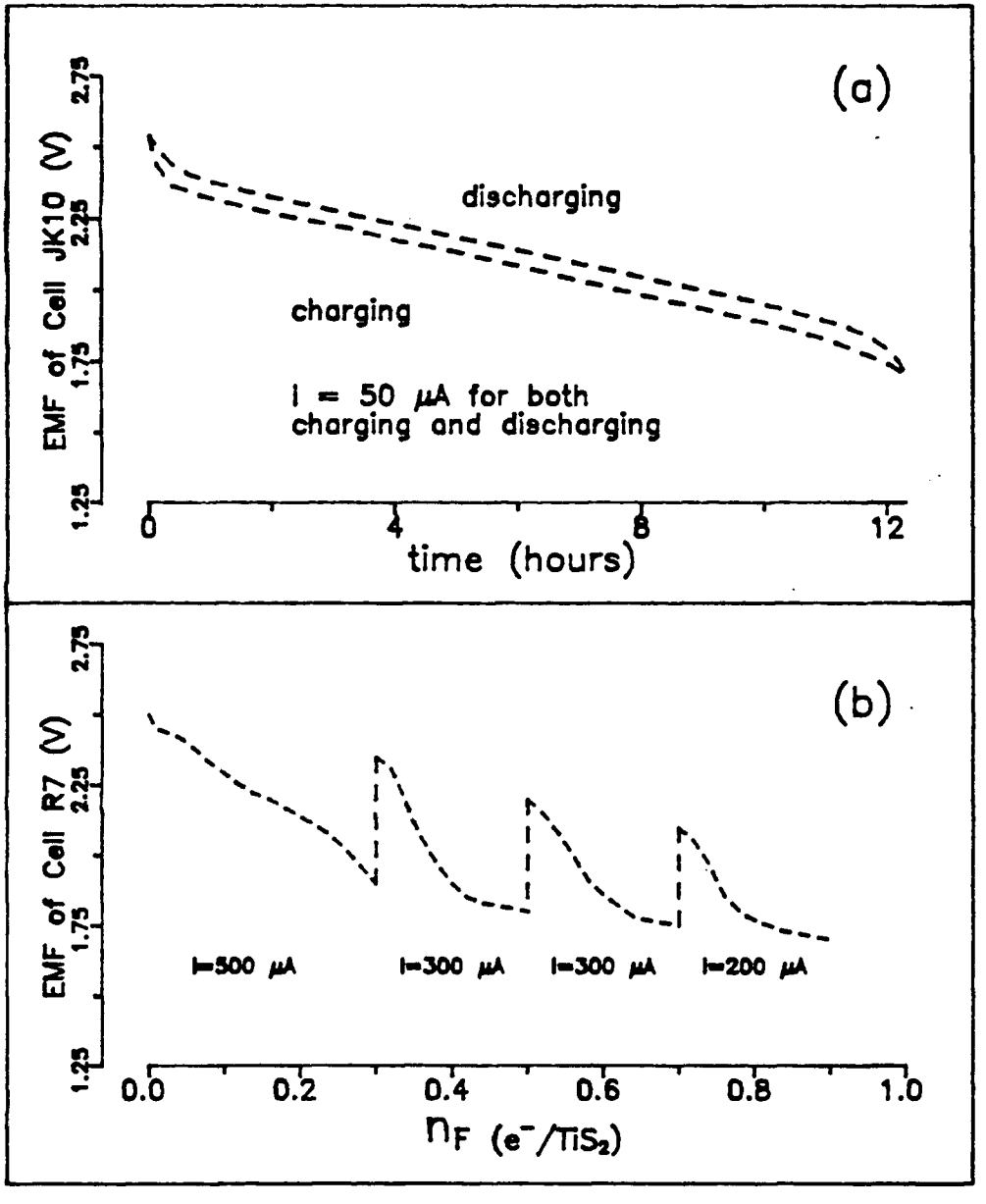

Figure 4.1: Cell EMF vs charge transport n_F. (a) The tenth continuous charge-discharge cycle of cell JK10. (b) Discontinuous first discharge of Cell R7, I=500 μA corresponds to an intercalation rate 4.73 hours.

region reduced and the voltage increases to a value which depends on the molar fraction of Li in Li_xTiS_2 compound as described in the references.

In future work, cell performance might be improved by using a large molecule electrolyte and adding carbon-black to the cathode material [17]. The large molecule electrolyte may prevent the co-intercalation process so that one does not need high current in the first discharge. A slow electrochemical process will allow intercalant metal to diffuse into the host properly and there will be no voltage jump in the open circuit cell. The carbon-black will serve as a good conducting mediator between crystalline grains to guarantee a homogeneous distribution of charge transfer into the entire host material.

4.2 Analysis of the TDPAC data

The quantity of physical interest, the pertubation factor, $G_{22}(t)$, was obtained from the raw correlation time spectra by the method described in section 3.4. For a given n_F the measurement was repeated 2 or 3 times to check the consistency of $G_{22}(t)$, and the final $G_{22}(t)$ was calculated from the weighted average of individual runs.

Each NQI is characterized by the following parameters : ν_q, the quadrupole interaction frequency; η, the asymmetry parameter and δ, the width of the interaction. By performing a discrete Fourier transform (DFT) on the perturbation function data, it was then possible to identify each static quadrupole interaction by its associated characteristic triplet in the frequency power spectrum. From the magnitudes of these frequency components and their ratios, initial values could be assigned for ν_q and η [12].

Fits to the G_{22} data were then performed using the program Minuit [18], with

$$G_{22}^{Theor} = \sum_i \alpha_i G_{22}^i(t) \tag{4.22}$$

where α_i are the fractional populations for each NQI ($\sum_i \alpha_i = 1$), and G_{22}^i represent static interactions of the form given in eq.(2.13). Since it was found (see section 4.3) that

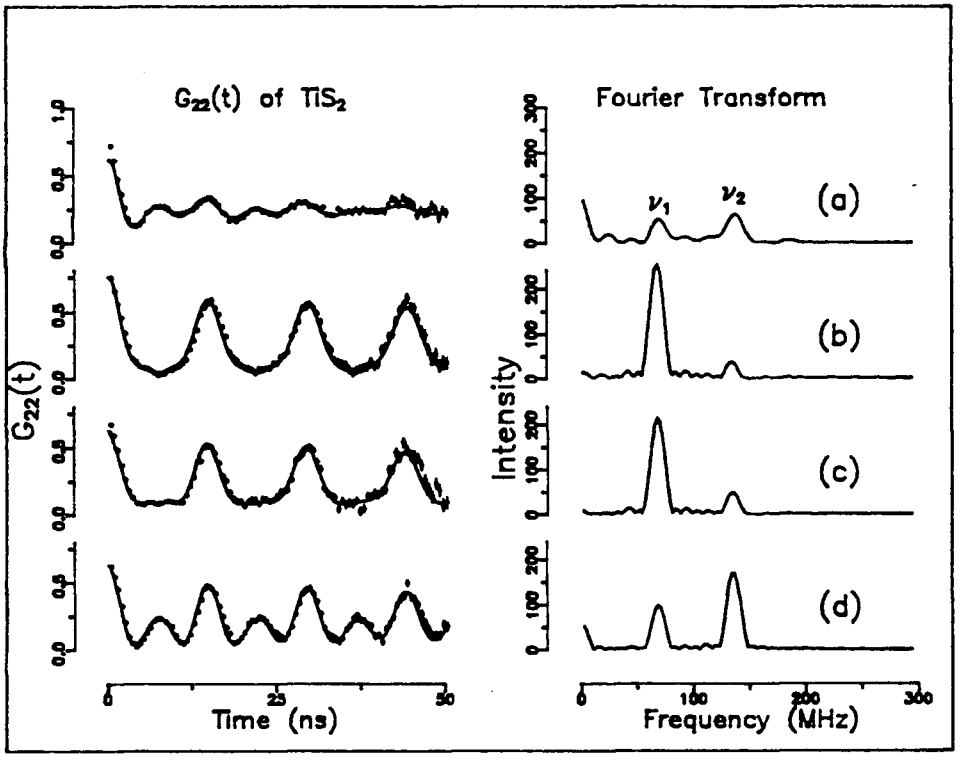

Figure 4.2: G_{22}(t) of ^{181}Hf in TiS_2 and their respective Fourier transforms : (a) sample without further treatment after being neutron irradiated; (b) the sample was annealed at 550 °C for 50 hours; (c) the sample was quenched in cool water after being annealed; (d) the annealed sample was placed in between two stainless steel flanges. Note that the frequencies ν_1 and ν_2 are not the quadrupole frequencies of the first and second interactions, but the first and second harmonics of the first interaction.

the samples clearly exhibited a preferential orientation, the S_n coefficients in eq. (2.13) were also allowed to vary in the fits. Thus, by minimizing χ^2 (chi squared) using the Minuit routine, the following best fit parameters to $G_{22}(t)$ were derived : $\nu_q, S_n, \omega_0, \eta, \delta$ and α_i.

4.3 Data for empty host TiS_2

Perturbation functions $G_{22}(t)$ of empty host TiS_2 in several conditions are presented in figure 4.14. The right side of figure 4.14 shows their respective Fourier power transforms. The latter indicate the presence of a well-resolved, static NQI. The fits to $G_{22}(t)$, however, require also the presence of a second, broadened NQI, which does not appear in the Fourier transforms. The well-resolved interaction is characterized by ν_q=456(4) MHz, $\eta = 0.06(3)$ and $\delta = 0.022(3)$ whereas the broadened interaction has a wide range of ν_q, η and δ. It should be recalled that for each interaction three frequencies should be observed for spin $\frac{5}{2}$. Owing to damping effects, however (see Chapter 3), the highest component of a given triplet is not always observed above the background.

The non-annealed sample produces poor results (see figure 4.14.a). The NQI in this case contributes only 16% to the total spectrum. Radiation damage may play an important role here, but the mechanism of the process is not fully understood.

Figures 4.14.b and 4.14.c represent annealed samples with and without quenching. The (b) sample was annealed at 550 °C for 50 hours and then cooled naturally by simply turning the furnace off. Sudden cooling was performed for sample (c), by placing the sample in cool water (t=15 °C) directly after 50 hours in the furnace. The time spectra of both samples are slighly different, but their Fourier transforms are almost identical to each other. The NQI contributes approximately 56% in both cases.

All three samples (a), (b) and (c) above are in the form of powders placed in pyrex tubes. For the purpose of electrochemical intercalation, each sample had to be placed in a sandwich comprising the substrate–sample–separator–Li foil, and the whole sandwich placed in between two stainlees steel flanges (see figure 3.2). An experiment performed to simulate the empty host sample in conditions similar to the Li_xTiS_2 described above gave results shown in figure 4.14.d. This can not be done after an actual Li/Li_xTiS_2 cell

Table 1: The fitting parameters of the well-resolved NQI of TiS_2

	Non annealed	Annealed	Quenched	Pressed
ν_q(MHz)	465(8)	452(4)	457(4)	454(4)
η	0.18(4)	0.06(3)	0.06(3)	0.08(3)
δ	0.044(8)	0.021(3)	0.0.027(3)	0.022(3)
% Contribution to the spectrum	15(2) %	56(2) %	55(2) %	45(2) %

has been constructed, since the cell has to be discharged immediately to avoid the co-intercalation process by solvent molecules, as described in the previous section.

The pressed sample[3] produced the same ν_q as the other empty host samples, but with different relative intensities for the individual frequency components. This phenomenon occurs because the pressed sample no longer represents a truly randomly oriented ensemble of microcrystallites, but shows a preferred orientation. This is reflected in the values of the S_n parameters; in the case of the annealed sample the S_1 and S_2 parameters are 0.481 and 0.224 respectively, whereas for the pressed sample S_1=0.256 and S_2=0.506. A list of the parameters of interest for the empty host samples can be seen in Table 1 for the well resolved static interaction. A discussion of the origin of the broad interaction is deferred to a later section.

[3]For simplicity the annealed TiS_2 sample placed in between stainless steel flanges is called a pressed sample.

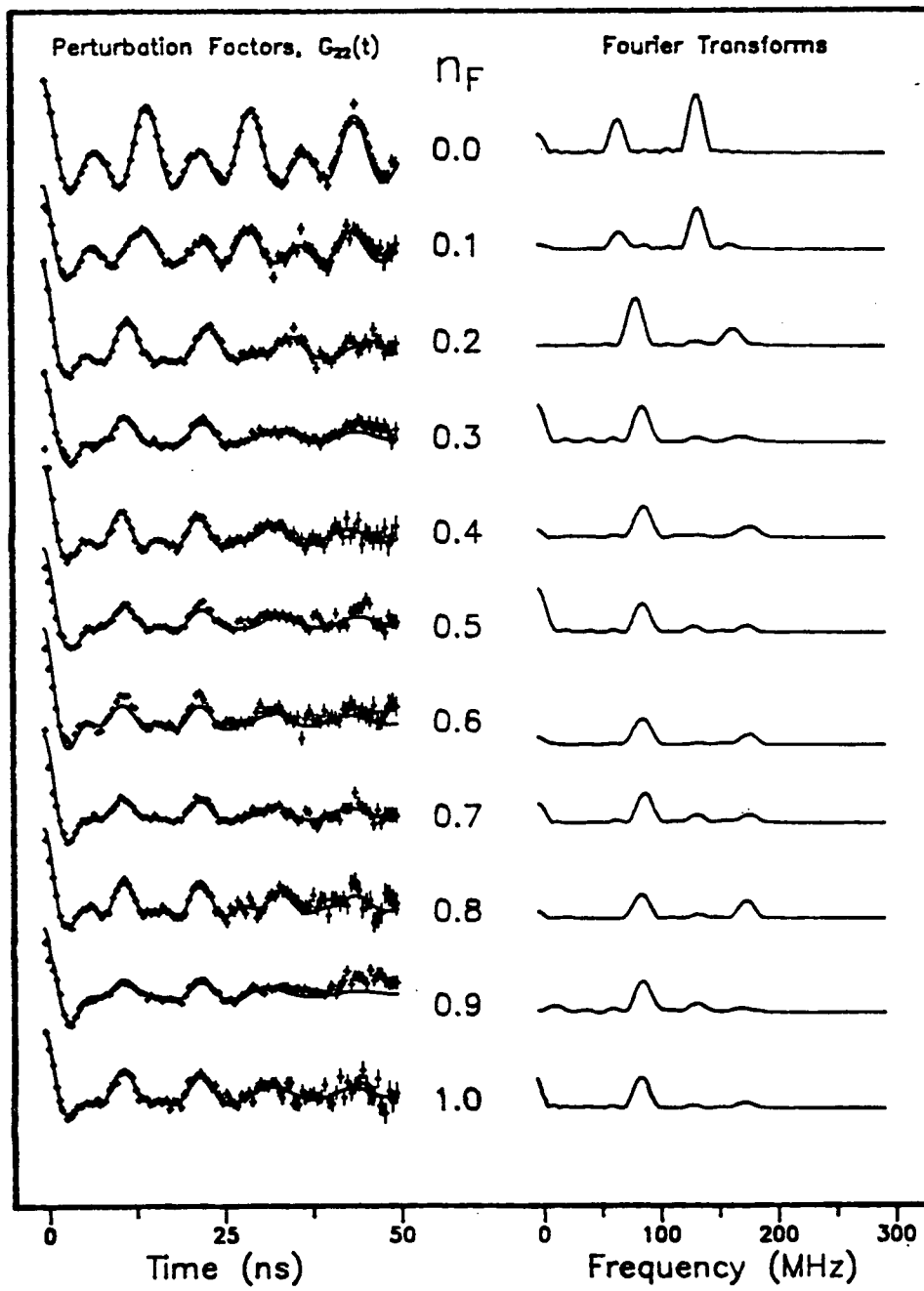

Figure 4.3: Perturbation factors, G_{22}, of ^{181}Hf in Li_xTiS_2 and their respective Fourier transforms.

4.4 Data for intercalated compound Li_xTiS_2

The perturbation functions $G_{22}(t)$ for intercalated compound Li_xTiS_2 and their respective Fourier transforms can be seen in figure 4.15. In this case it was found that equation (4.22) required three interactions in order to obtain reasonable fits. Table 2 lists the parameters obtained from the fits for the NQI of interest.

Table 2: Fitting parameters of Li_xTiS_2

	First Interaction				Second Interaction			
n_F	η_1	δ_1	ν_{q1} (MHz)	%	η_2	δ_2	ν_{q2} (MHz)	%
0.0	.08(3)	.022(3)	454(4)	45(2)	–	–	–	–
0.1	.09(3)	.024(4)	460(5)	21(2)	.14(4)	.061(5)	568(5)	19(2)
0.2	.19(4)	.076(5)	460(5)	15(2)	.12(4)	.054(5)	568(5)	44(3)
0.3	.12(4)	.082(6)	451(5)	11(2)	.15(4)	.064(5)	587(5)	27(3)
0.4	.29(4)	.108(5)	451(5)	12(2)	.14(4)	.050(5)	608(6)	36(3)
0.5	.23(3)	.094(5)	453(5)	16(2)	.09(3)	.064(6)	595(5)	36(3)
0.6	.27(3)	.102(5)	477(5)	15(2)	.14(4)	.054(5)	606(6)	43(3)
0.7	.22(3)	.092(5)	456(5)	15(2)	.14(4)	.058(5)	602(6)	30(3)
0.8	.27(3)	.066(5)	480(5)	14(2)	.12(4)	.040(4)	599(5)	38(3)
0.9	.00(3)	.066(5)	448(5)	14(2)	.18(4)	.094(6)	589(6)	32(3)
1.0	.17(3)	.057(5)	451(5)	11(2)	.14(4)	.069(6)	597(5)	40(3)

There are two well defined static interactions of narrow width : the first one is the empty host NQI, whose contribution decays rapidly in the range $0 \leq x \leq 0.2$, thereafter remaining constant; the second interaction increases slowly in the region $0 < x < 0.2$, becoming dominant for $x > 0.2$. The third interaction contributes approximately 40%–60% to the spectrum. It is similar to the second interaction found in the empty host case i.e. characterized by a small asymmetry parameter η, a large δ and large scatter in ν_q. This interaction was introduced in order to get satisfactory fits. As will be pointed

out in the discussion of Chapter 5, although the presence of this interaction is a useful indicator of sample quality, it is not of great interest theoretically.

Figure (4.16) summarizes the results of the TDPAC measurements on the Li_xTiS_2 system. Here we depict the variation of the fit parameters with n_F for the two interactions of interest. The quadrupole frequency ν_q is presented in figure 4.16.a. The first interaction produces a more or less constant frequency with average $\overline{\nu_{q1}} = 461(5)$ MHz. The second interaction reveals itself at $x \approx 0.1$ with a 19% contribution and becomes dominant at $x \approx 0.2$ at the 44% level. Its frequency stays constant below x=0.2, then increases in the region $0.2 < x < 0.4$, remaining constant beyond x=0.4 with $\overline{\nu_{2q}}$=599(6) MHz. The relative change in the populations of interactions 1 and 2 is presented in figure 4.16.b, treating the broad, non-specific third interaction as a background which can be subtracted. It can be seen that while the empty host population decreases at the expense of the second NQI, it does not decay to zero. Finally in figure 4.16.c and 4.16.d we show the variation of δ with n_F. In both interactions δ is essentially constant, although δ_1 falls off slightly in the region $0 < x < 0.3$.

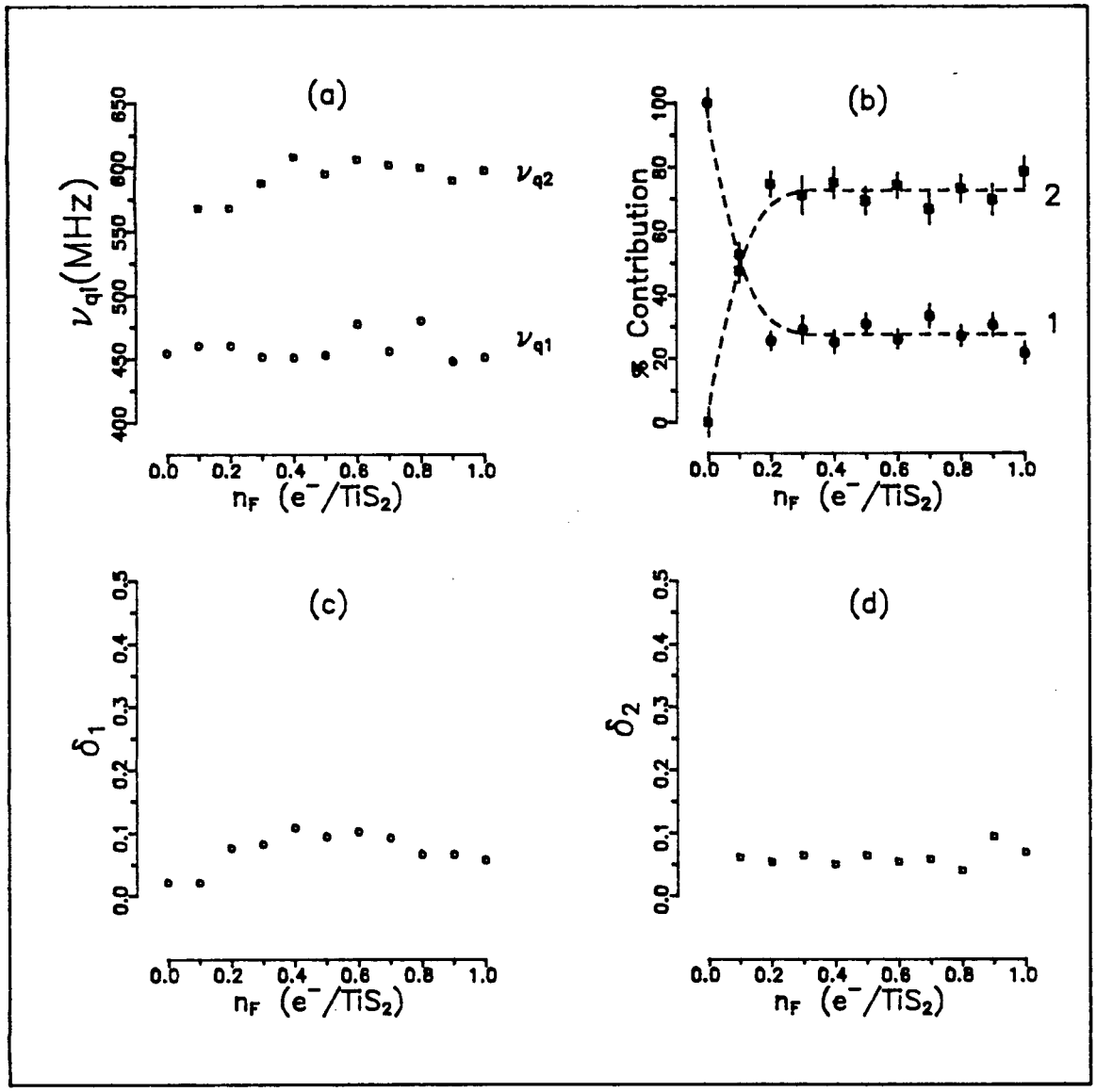

Figure 4.4: The dependence of fit parameters on the charge transport, n_F. Note: The dashed lines in (b) are aids to the eye. The error bars in (a), (c) and (d) lie inside the data points.

Chapter 5

Discussion

5.1 Introduction

The work of Butz and his colleagues [19-22] has shown that TDPAC spectroscopy is a powerful tool in elucidating the intercalation mechanism. Studies of Li_xTaS_2, Ag_xTaS_2 and Li_xZrS_2, for example, have shown that TDPAC can reveal the sequence of intermediate phases formed during intercalation and their intercalate packing density. Especially important was the finding that the nuclear quadrupole frequency was directly related to p, the local intercalate packing density of lithium atoms [21], so that even variations in p within the same layer can be detected. There is almost no possibility to detect this using X-ray or neutron scattering techniques.

Thus the observation of sharp, discrete quadrupole frequencies and their variation in magnitude and intensity as a function of n_F provides a key to the interpretation of the intercalation process.

5.2 Cathode utilization

Cathode utilization represents the percentage of cathode material involved in the electrochemical reaction. Poor electrical contact can occur between the cathode material and the substrate [6], as a result of which not all of the cathode material can be intercalated. A certain fraction of the host material remains unchanged. By definition cathode utilization of a cell must be less than or equal to 100%. In the following section

we discuss the cathode utilization in this work and how it can be determined.

Cathode utilization of a cell is usually determined from its cycling performance (charge–discharge cycle). A cell having cathode utilization less than 100% gives shorter cycles than that of an ideal cell. Numerically it can be calculated using the equation:

$$U = \frac{n_F}{x} \times 100\%. \tag{5.23}$$

The molar fraction x is determined by measuring the voltage of the cell V(n_F) and then inferring x from calibrated measurements of V(x) in the literature [1,7]. The charge transport n_F is determined from eq.(1.4) by measuring the time and current of the reaction.

In our case, however, this method is not readily applicable, owing to the discontinuous nature of the discharge process, as mentioned in Chapter 4. Instead, the TDPAC data can be used to infer the cathode utilization factor directly from the fact that an empty host interaction persists even until n_F=1.0. Assuming a homogeneous distribution for the Hf probe, this signal must represent regions of the crystal structure unavailable to the intercalating Li atoms. The data in figure 4.4.b. indicate an empty host component, $f_{EH} = 27.9 \pm 3.5\%$, yielding a cathode utilization factor in the region of 70–80%, comparable with that quoted by Thompson [7].

5.3 The Nuclear Quadrupole Interaction in Li_xTiS_2

5.3.1 The broad, non-specific interaction

In both the empty host TiS_2 and Li_xTiS_2 samples the TDPAC spectra showed evidence for a broad, non- specific interaction characterized by a wide range of ν_q and δ. We speculate that there are two possible sources for this interaction.

One possibility is that this signal originates from ^{181}Hf probe atoms which have not substituted for Ti atoms in regular lattice sites. Such atoms could, for example,

be trapped at crystalline grain boundaries, where a wide variation in the efg could be expected. The dramatic improvement of the time spectra following the annealing process (see figure 4.2) lends support to this conjecture. In the annealed sample the fractional population corresponding to this interaction is reduced by almost a factor of 2.

The fact remains, however, that even after annealing a significant fraction of sites ($\approx$ 40%) still exhibit these features. This suggest that another mechanism must be present which is basically unaffected by the annealing process. Such an effect could be produced by co-intercalation of the PC solvent. This occurs when lithium ions are intercalated into the host along with a PC solvation cloud. In fact the term *intercalation* here is a misnomer, in the sense that the changes in the host lattice are quite drastic and irreversible. Instead we refer to this process as PC *insertion* [6]. It is believed that solvent insertion can be avoided by using less polar solvents [17]. Because of its high sensitivity, TDPAC will be an excellent vehicle to check this hypothesis, and this will be on the agenda for future experiments. Thus TDPAC may be able to play a significant role in quality control analysis for the testing of new materials in electrochemical cells.

5.3.2 The well resolved, specific Nuclear Quadrupole Interaction

Figure 4.4.b indicates that 27.9% of the cathode material is not involved in the electrochemical reaction and remains unchanged. Since the intercalation of available sites should be complete by n_F=1, any residual empty host contribution at this value of n_F must represent those regions of the material inaccessible to intercalating Li atoms. Hence, in order to obtain the true growth and decay of the NQI for the crystalline material involved in the intercalation process, the residual empty host signal at large n_F should be regarded as the zero level and consequently the contributions represented in fig. 4.4 (b) should be rescaled. This gives rise to the relative contributions depicted in fig. 5.1, which shows the growth and decay of the NQI frequencies in sites available for intercalation.

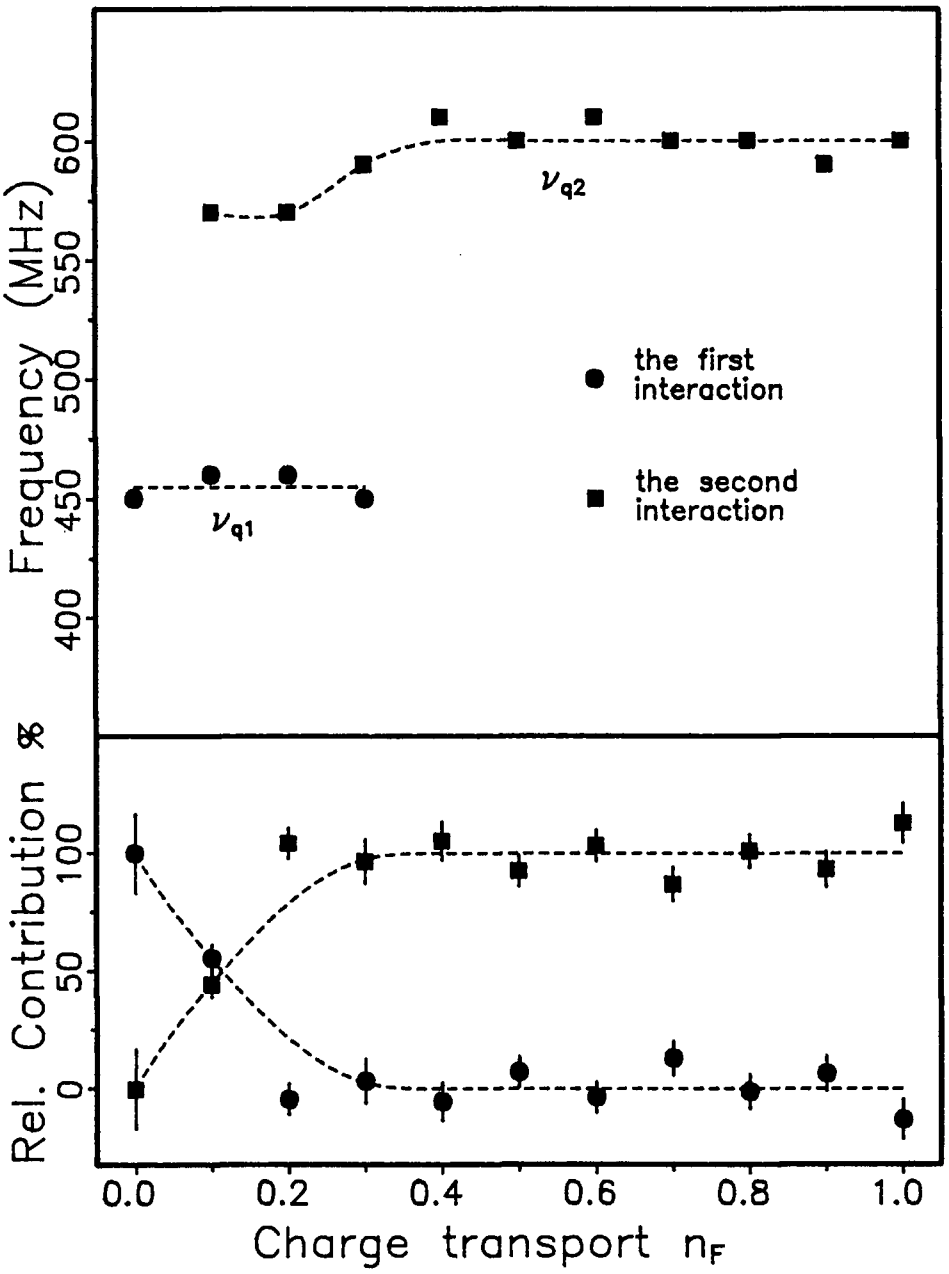

Figure 5.1: Nuclear quadrupole frequencies and percent contribution of the first (solid circles) and second (open circles) interactions vs. n_F after subtraction of residual empty host background. This represents the behaviour in regions of the crystal accessible to intercalating Li atoms. Note: the error bars of the frequency curves are contained in the data points.

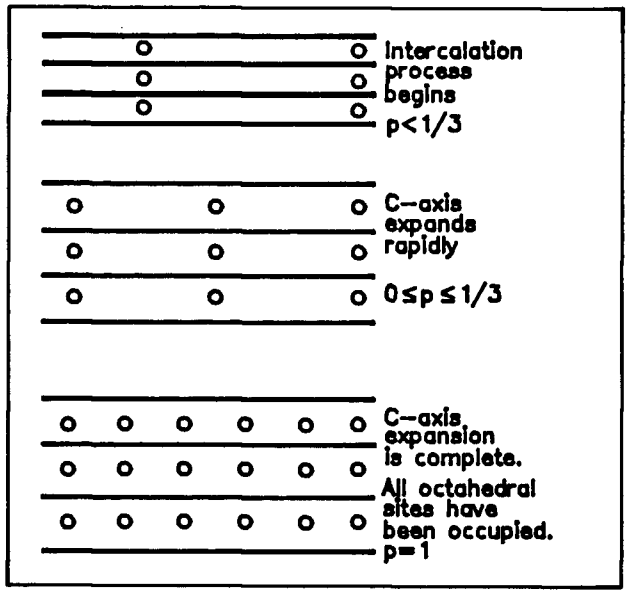

Figure 5.2: A model of $Li \rightarrow TiS_2$ intercalation process. The circles and horizontal lines represent Li atoms and TiS_2 sandwiches respectively.

The molar fraction behaviour is very similar to that obtained for Li_xZrS_2 by Lerf and Butz [23], where the empty signal disappears after $n_F \approx 0.3$. On the other hand, in our case the NQI frequency for the lithiated regions, ν_{q2}, is higher, as opposed to lower, than the empty host signal, ν_{q1}, and ν_{q2} shows a gradual increase in the region $0 < n_F < 0.3$ before attaining the constant value of $\approx$ 600 MHz. In the interval $0 < n_F < 0.3$, where the c–axis expands rapidly [6,24], the behaviour of ν_{q2} indicates that the local packing density of Li atoms, p, slowly increases to a maximum, steady value. This may still be consistent with the finding of Thompson [7], who suggested that ordering can occur in a two-dimensional superlattice in the Li_xTiS_2 for $x = 1, \frac{1}{3}, \frac{1}{4}, \frac{1}{7}, \frac{1}{9}, \cdots$. Owing possibly to the high initial lithium current densities, the lower Li packing densities are not resolved in the TDPAC measurements, consequently initial values are smeared out and only the limiting value p=1 is observed. This implies that the NQI is extremely localized, determined almost solely by the charge transfer to surrounding sulphur atoms.

Figure 5.18 demonstrates a model for the intercalation process. As the c–axis expands, p increases to its maximum value of 1, thereafter remaining constant.

Unfortunately it is not feasible to make a realistic calculation of the efg in such a complex system as Li_xTiS_2, since little is known about the electronic wave functions and band structure, particulary for the Hf-doped compound. From other measurements [7] we know that in the range $0 \leq x \leq 1$ only octahedral sites are occupied. The NQI parameters obtained from the fits are consistent with such an assignment.

Chapter 6

Conclusion

In the high current electrointercalation of Li in TiS_2 two nuclear quadrupole interactions, consistent with octahedral symmetry, are observed in the region of charge transport $0 \leq n_F \leq 1$. The first interaction originates from empty host material (p=0). It is characterized by a constant quadrupole frequency with average $\overline{\nu_{q1}}$=461(5) MHz. The quadrupole frequency of the lithiated TiS_2 (Li_xTiS_2) shows a gradual increase in the low n_F region, $0 \leq n_F \leq 0.3$, and then attains a constant value of $\overline{\nu_{q2}}$=599(6) MHz for $0.3 \leq n_F \leq 1$. The second interaction corresponds to a compound which rapidly reaches a high packing density of Li (p=1).

TDPAC provides a sensitive tool for assessing material quality in electrochemical cells. The cathode utilization factor is readily determined from the size of the residual empty host signal; microcrystalline imperfections are revealed as NQI frequencies with large δ.

In addition TDPAC demonstrates the necessity for annealing the sample following neutron irradiation. Quenching of the samples appears to make little difference to the results.

Further work which may be performed should include :

- Improvement of battery performance so that a slow intercalation process can be performed. This may involve
  - Using other electrolytes so that co-intercalation processes can be avoided.

  - Adding conductive material to the sample to improve electrical conduction between substrate and crystalline grains and between crystalline grains themselves. This might improve cathode utilization.

- TDPAC measurements in the low n_F region. The region $0 \leq x \leq 0.4$ seems to be very sensitive to variations in n_F.

- Temperature dependence of the intercalation process.

The above mentioned work should greatly improve our understanding of metal intercalation into layered compounds.

Bibliography

[1] M. S. Whittingham, Prog. Solid State Chem., **12** (1978), 41.

[2] C. Ramos, A. Lerf, S. Saibene and T. Butz, Solid State Ionics, 31, (1988), 177.

[3] Peter J. Mulhern, *Lithium Intercalation in Crystalline* Li_xMoS_2, PhD. Thesis, Department of Physics, Univ. of B. C., (1986).

[4] J. R. Dahn, D. C. Dahn and R. R. Hearing, Solid State Comm., **42**, 3, (1982), 179.

[5] M. Inoue, H. P. Hughes and A. D. Yoffe, Advance in Physics, **38**, 5, (1989), 565.

[6] J. R. Dahn, *Lithium Intercalation in Titanium Disulphide*, MSc. Thesis, Dept. of Physics, Univ. of British Columbia, Canada, (1980).

[7] A. H. Thompson, Phys. Rev. Let., **40**, 23, (1978), 1511.

[8] A. H. Thompson and F. R. Gamble, Mat. Res. Bul., **10**, (1975), 915.

[9] M. S. Whittingham and F. R. Gamble Jr., Mat. Res. Bul., **10**, (1975), 363.

[10] M. B. Dines, Mat. Res. Bul., **10**, (1975), 287.

[11] W. R. McKinnon, Solid State Comm., **40**, (1981), 343.

[12] H. Frauenfelder and R. M. Steffen, in *Alpha-, Beta-, and Gamma-, Spectroscopy*, ed. K. Siegbahn, North Holland Publishing Co., Amsterdam, (1965).

[13] M. E. Rose, Phys. Rev., **91**, (1953), 610.

[14] P. W. Martin and S. El-Kateb, J. Chem. Phys., **76**, (1982), 3819.

[15] J. R. Dahn and W. R. McKinnon, J. Phys., **17**, (1984), 4231.

[16] T. Hibma, Physica, **99B**, (1980), 136.

[17] J. R. Dahn, private communication.

[18] F. James and M. Roos, Comp. Phy. Com., **10**, (1975), 343.

[19] T. Butz and A. Hubler, Mat. Res. Bul., **16**, (1981), 541.

[20] T. Butz, A. Vasquez, H. Saitovitch, G. M. Kalvius, and A. Lerf, Hyp. Int., **4**, (1978), 978.

[21] T. Butz, A. Lerf, Ber. Bunsenges. Phys. Chem., **90**, (1986), 638.

[22] A. Lerf and T. Butz, Angew. Chem. Int. Ed. Engl., **26**, (1987),110.

[23] A. Lerf and T. Butz in Reactivity of Solids edited by P. Barret and L. C. Dufour, Elsevier Science Publiser B. V., Amsterdam, (1985), p 493.

[24] Whittingham, F. R. Gamble and C. R. Simon, Mat. Res. Bul., **10**, (1978), 363.